Toxic metal sequential sequestration in water using new amido-aminoacid ligand as a model for the interaction with polyamidoamines

Toxic metal sequential sequestration in water using new amido-aminoacid ligand as a model for the interaction with polyamidoamines

Laura Bergamonti[a,*], Silvia Gentili[a], Domenico Acquotti[b], Matteo Tegoni[a], Pier Paolo Lottici[c], Claudia Graiff[a,**]

[a] Department of Chemistry, Life Science and Environmental Sustainability, University of Parma, Parco Area delle Scienze 17/A, 43124 Parma, Italy

[b] Centro di Servizi e Misure, University of Parma, Parco Area delle Scienze 23/A, 43124 Parma, Italy

[c] Department of Mathematical, Physical and Computer Sciences, University of Parma, Parco Area delle Scienze 7/A, 43124 Parma, Italy

* Corresponding author. E-mail address: laura.bergamonti@unipr.it

** Corresponding author. E-mail address: claudia.graiff@unipr.it

Abstract

Polyamidoamines are low cost and easily synthesized materials that may find applications in cations sequestration and water treatment. In this paper a new amido-aminoacid ligand containing methionine has been designed as a monomeric model of the corresponding polyamidoamine. The amido-aminoacid ligand has been synthesized in high yield, by reacting acrylamide and methionine *via* aza-Michael addition in water and mild temperature conditions. The reaction has been monitored by NMR and Raman spectroscopies and the crystal structure has been determined by X-ray diffraction analysis. The coordination ability of the ligand towards Cu^{2+} cations in water, as well as its affinity for Ni^{2+} and Co^{2+} has been studied by potentiometric and spectrophotometric techniques. The divalent metal cations sequestration from water may occur with sequential selection by changing the pH of the solution. The copper complex with two coordinated ligands has been fully characterized in the solid state by single crystal X-ray diffraction. The results are discussed with a view to use these materials in the treatment of water contaminated by toxic transition metal ions.

Keywords: Sequential sequestration of transition metals; Amido-aminoacid ligand; Methionine; Complex-formation equilibria; Wastewater treatments

1. Introduction

In the last decades, toxic heavy metals contamination in aqueous systems has become a global environmental problem due to the harmful effects towards living organisms. Even at trace levels these metals can cause ecological and health damages, due to their high toxicity, high solubility, migration activity and stability in aqueous media and bioaccumulation tendency (Zheng et al., 2020; Essaimi et al., 2012; Xiaoli et al., 2007; Marcovecchio, et al. 2007). High level of toxic heavy metals concentration in water, as colloidal, particulate and dissolved phases, can originate from both natural (volcanic eruption and rock weathering) and anthropogenic sources (solid waste disposal and agricultural, industrial or

domestic effluents) (Nasir et al., 2019; Vareda et al., 2019). The main toxic heavy metals found in aqueous solutions are Cu, Cd, Hg, Pb, Ni and Zn (as divalent ions) and Cr, As and Se (multivalent ions) (Vardhan et al., 2019; Malik et al., 2019).

To remove toxic metal ions from water systems, several processes have been proposed: photocatalysis, electrochemical treatments, chemical precipitation, ion exchange, adsorption, coagulation-flocculation, membrane filtration, bioremediation (Betiha et al., 2020; Tahir et al., 2019; Brahmi et al., 2018; Alberti et al., 2018; Lee et al., 2016; Rezania et al., 2016; Fu and Wang, 2011; Pan et al., 2007). Among these methods, adsorption is one the most efficient techniques thanks to the easy tuning for different targets, versatility in design, low cost and recyclability for multiple re-use (Wadhawan et al., 2020; Zhou et al., 2018; Lakherwal et al., 2014)

Many efforts have been made to develop highly selective non-toxic and biocompatible adsorbent materials (Bo et al., 2020; Joseph et al., 2019; Li et al., 2018; Uddin, 2017; Febrianto et al., 2009; Bailey et al., 1999). The effectiveness in removing heavy metals from contaminated aqueous media depends on the density of adsorption sites and on the capacity to strongly link metals. Chelating agents containing amines and carboxylate groups, such as aminoacids, aminopolycarboxylic acids and polyamidoamines are known to form stable structures with metal cations (Wang et al., 2020; Nasir et al., 2019; Ju et al., 2019; Lachowicz et al., 2018; Bergamonti et al., 2017a; Tarazona-Vasquez and Balbuena, 2005).

Polyamidoamines (PAAs) are a class of biocompatible and biodegradable linear or cross-linked polymers which can be functionalized, for example with hydroxyl, carboxylic or siloxane groups, for several applications (Bergamonti et al., 2017b; Girardi et al., 2016; Isca et al., 2016; Zintchenko et al., 2011; Ferruti et al., 2002). PAAs, in free-linear, cross-linked and silica-grafted forms, are able to coordinate transition metal ions, namely Cu^{2+}, Ni^{2+}, Co^{2+} (Bergamonti et al., 2019; Casolaro et al., 1998; Ferruti et al., 1980): the formed complexes are stable in water as proved by potentiometric and spectroscopic studies (Bergamonti et al., 2017a; Tarazona-Vasquez and Balbuena, 2005; Xu and Zhao, 2005; Ferruti et al., 1981; Barbucci et al., 1980). These results suggest the use of polyamidoamines as

inorganic pollutants sorbing materials for wastewater purification (Manfredi et al., 2013; Ferruti et al., 2012).

PAAs are prepared by addition reaction between bisacrylamide and amines or aminoacids (Ferruti, 2013). This is known as aza-Michael addition and is regarded as a green reaction due to the use of water as solvent, the mild temperature conditions and the absence of added catalysts.

Among the aza-Michael additions, the use of aminoacids as source of amines for the PAAs synthesis has been scarcely investigated (Manfredi et al., 2017; Ferruti et al., 2014). Some studies of model amidoamines in monomeric form derived from aminoacids have been reported (Nehls et al., 2013; Chandrarekha et al., 2015) and few examples on the capability of these molecules to coordinate metal cations (Rajalakshmi et al., 2008; Lim et al., 1994) have been described. Nevertheless, the use of aminoacids allows the introduction, in the polymeric structure, of carboxylate functions which may be significant in determining stable coordination of metal ions, and subsequent higher efficiency to strongly adsorb metals.

Here we have characterized by spectroscopic and diffractometric methods the product of acrylamide with methionine (AcryMet) as a monomeric molecular model of the corresponding polyamidoamine. The coordination ability of this monomer toward Cu^{2+} and, for the sake of comparison, toward Co^{2+} and Ni^{2+}, has been evaluated in aqueous solution by studying their speciation models.

The results obtained for the AcryMet model are the starting point to assess the metal coordination ability of the corresponding polymer for its use as specific absorber of heavy metal ions for water purification. In particular, we will show here that AcryMet is able to form complexes with Cu^{2+}, Ni^{2+} and Co^{2+} in different pH ranges. This behavior may be used to differentiate metal ions on the basis of their sequential binding to these ligands and their polymers as the pH of the medium increases from acidic to neutral.

2. Experimental Section

2.1 Materials

Acrylamide (98%), L-methionine (99.9%), copper (II) acetate (99%), nickel (II) acetate, cobalt (II) acetate, DMSO-d_6 were purchased from Sigma-Aldrich and used as received. Concentrated sodium hydroxide and Titrisol$^{@}$ solutions were purchased by Merck.

2.2 Synthesis of 3(2-amino-4-(methylthio)butanoic acid)propanamide (AcryMet).

A water solution of pure L-methionine was added to a water solution of acrylamide in equimolar ratio in presence of ammonium buffer solution (pH=10.6). The reaction mixture was stirred at 70 °C for 4 hours and then the solvent was evaporated in vacuum to give the crude product (yield: 99%) as a white microcrystalline powder. The powder was then re-dissolved in water and, after a slow evaporation of the solvent at 4 °C, colorless crystals with a needle aspect of AcryMet were obtained, suitable for X ray diffraction analysis.

2.3 Reaction of AcryMet with copper acetate. Synthesis of Cu-AcryMet complex

A water solution (15 mL) of AcryMet (0.176 g, 0.8 mmol) was added dropwise to a water solution (15 mL) containing $Cu(CH_3COO)_2 \cdot H_2O$ (0.080 g, 0.4 mmol). The blue solution was stirred at room temperature for 1 hour. Then the solvent was allowed to evaporate. The solid residue was re-dissolved in water and, by slow crystallization using acetone as non-solvent, blue single crystals were obtained (Yield 70%).

2.4 Nuclear Magnetic Resonance

^{1}H NMR spectra were recorded in a spectrometer JEOL ECZ600R operating at 600.17 MHz using a 5 mm multinuclear probe for high resolution with actively shielded gradient along the z-axis, equipped for automatic tuning and matching. The acquisition of spectra was carried out using solutions of about 75 mg of the compound dissolved in 0.6 mL of deuterated solvent. The probe temperature was 318 K for all spectra. The solvents used was DMSO-d_6, used also as internal reference. The complete characterization

was done running 1D ^{1}H and ^{13}C DEPT spectra, 2D homonuclear COSY, TOCSY and heteronuclear HSQC and HMBC spectra.

The typical operation conditions for the 1D proton spectra were: 18063.58 Hz spectral width with 64 K data points, 32 scans: Acquisition time and repetition time were 3.63 and 6.63 sec, respectively.

Gradient-selected gCOSY (Hurd, 1990) spectra were obtained with 4096 data points covering a spectral width of 9.0058 kHz in both dimensions. Two scans were acquired for each of 256 increments, with an acquisition time of 0.568 s and a relaxation delay of 1.5 s.

TOCSY spectra (Levitt et al., 1982) were acquired with a spinlock time of 80 ms, with the same experimental parameters reported for gCOSY. Four scans were done for each of 256 increments, with an acquisition time of 0.455 s and a relaxation delay of 1.5 s.

Gradient-selected HSQC spectra (Wilker et al., 1993) were obtained with the same experimental parameters reported for TOCSY in F2 and a spectral width of 25.668 kHz in F1.

The gradient selected heteronuclear multiple bond correlation spectra HMBC (Rinaldi and Keifer, 1994) were obtained in the same conditions, with spectral widths of 37.764 kHz in F1.

2.5 Raman Spectroscopy

Raman spectra were acquired at 632.8 nm in backscattered geometry with a Horiba - Jobin Yvon LabRam micro-spectrometer (300 mm focal length) equipped with an integrated Olympus BX40 microscope. The spectral resolution was about 1.5 cm^{-1}. The laser power on the samples was adjusted by means of density filters to avoid uncontrolled thermal effects and always kept less than 1 mW. Spectra were collected using a long working distance x50 microscope objective. Typical exposures were 60-90 s, with 3-5 repetitions.

2.6 Potentiometric studies

The potentiometric titrations of ligand AcryMet (HL) were carried out in aqueous solution at T = 298.2 ± 0.1 K and I = 0.1 M (KCl) under N_2 stream, using 20 mL samples. The potentiometric apparatus

was previously described (Quaretti et al., 2018). The Hamilton combined glass electrode (P/N 238000) was calibrated in terms of [H^+] by titrating HCl solutions with a 0.14 M carbonate-free standardized solution of KOH and the pK_w value resulted to be 13.76(1). Protonation data were obtained by alkalimetric titration of 3 samples (C_{Ligand} = 2.8-8.8 10^{-3} M). Formation constants of the complexes with the divalent metals Cu^{2+}, Co^{2+}, Ni^{2+}, and Zn^{2+} (M^{2+}) were determined by alkalimetric titration of 3 samples (C_{Metal} = 0.65-1.8 10^{-3} M; L:M = 1.5-4.2). Systems containing Cu^{2+} and Ni^{2+} were studied between pH 2.5 and 11. Systems containing Co^{2+} and Zn^{2+} were limited to the pH range 2.5-9 and 2-8, respectively. For the latter two systems, drift in the e.m.f. and opalescence was observed at higher pH.

The protonation and complex-formation constants of the systems were calculated with HyperQuad 2013 software (Gans et al., 1996) and the results were used to draw the species distribution curves with Hyss 2009 program (Alderighi et al., 1999).

2.7 UV-visible spectrophotometry

UV-visible spectra of the Cu^{2+}/AcryMet; Ni^{2+}/AcryMet and Co^{2+}/AcryMet systems were collected with an Evolution 260 Bio (Thermo Scientific, Waltham, MA, USA) spectrophotometer provided with a Peltier thermostat, using quartz cuvettes of 1 cm path length. Solutions containing the ligand (L) and the metal (M) were prepared under inert atmosphere (C_L= 5-5.5 10^{-3} M, M:L = 2.2 for Cu^{2+}, or 4.2 for Co^{2+} and Ni^{2+}; total volume 20 mL). The pH was adjusted to selected pH values by additions of standard KOH titrant, the solution transferred in the cuvette and the spectrum collected in the 250-900 nm range. The range of pH was 2.1-11.2 for Cu^{2+}, 3.2-10.8 for Ni^{2+}, and 3.2-8.9 for Co^{2+}. At higher pH values, turbidity in the solutions of Ni^{2+}/AcryMet and Co^{2+}/AcryMet was observed. UV-visible spectrophotometric titration data for the Cu^{2+}/AcryMet system were analysed with the HypSpec 2014 program (Gans et al., 1996).

2.8 Metal ion adsorption

The metal ions adsorption capacity of Acry-Met ligand was determined by UV-Vis adsorption spectrophometry. To perform the adsorption experiments, the Acry-Met ligand was dispersed on a TEOS

(Tetraethyl orthosilicate) film prepared via sol-gel in basic medium: 0.9 g of Acry-Met (4.1 mmol; pH = 9.6) was dissolved in 5 ml of water and added to a TEOS solution, previously prepared solving 3.2 ml of TEOS in 5 ml of ethanol; the resulting solution was cast in a Petri disk and left drying at room temperature 24h to obtain the film; the film was equally cut in three part. Then, 20 ml aqueous solutions (0.0125 mol/L) of Cu (II), Co (II) and Ni (II) were prepared starting from metal acetates. Acry-Met ligand film was added to every metal ion solution, obtaining Lig/M^{2+}= 5:1. The initial pH of the solutions was adjusted with 0.1 M HCl (pH_{Cu} = 4.5, $pH_{Co,Ni}$ = 6). At defined time intervals, 0.5 ml of solution were taking and filtered (pore size 0.45μm). Absorbance of metal ion solution was determined at the maximum absorption wavelength (712 for Cu(II), 514 nm for Co(II) and for Ni(II)) by UV–Vis. The experiments were carried out at room temperature. Adsorption experiment, as a blank correction, was performed on pure TEOS film.

To determine the adsorption capacity (adsorption uptake rate) of adsorbent at equilibrium, q_e (mg/g), and the removal percentage, R_{ads} (%), due to adsorption of metal ions, the following equations was used:

$$q_e = \frac{C_0 - C_e}{w} V \qquad (1)$$

$$R_{ads}\,(\%) = \frac{C_0 - C_e}{C_0} 100 \qquad (2)$$

where C_0 (mg/L) and C_e (mg/L) are the initial and equilibrium concentration of metal solution, respectively. V (ml) is the volume of adsorbate solution and w (g) is the weight of adsorbent.

2.9 X-ray Data Collection, structure solution and refinement of AcryMet and Cu^{2+}/AcryMet complex.

X-ray crystallographic data of AcryMet and *Cu^{2+}/AcryMet* complex were obtained on single crystals with an APEX 2 Bruker CCD diffractometer. The APEX 3 program package (Bruker, 2015) was used for the data collection (30 s/frame scan time for a sphere of diffraction data) and to determine the unit-cell parameters. The structures were solved using SHELXT (Sheldrick, 2015) by Intrinsic Phasing method in the APEX 3 program. Subsequent calculations were carried out using the SHELXTL-2014/7 program in the WinGX suite v.2014.1 (Farrugia, 2012). The refinement was carried out based on F^2 by full-matrix least-squares techniques. Crystallographic data have been deposited with the Cambridge Crystallographic Data Centre as supplementary publication. Copies of the data can be obtained free of charge on application to the CCDC, 12 Union Road, Cambridge CB2 1EZ, U.K. (fax, (+44) 1223 336033; e-mail,

deposit@ccdc. cam.ac.uk). Deposition Number CCDC 2023768 and 2023769 for AcryMet and Cu^{2+}/AcryMet respectively.

3. Results and Discussion

3.1 NMR and Raman spectroscopic characterization of AcryMet.

The addition between acrylamide and L-methionine in equimolar ratio leads to the formation in high yield (99 %) of the AcryMet adduct, whose structure is reported in Scheme 1.

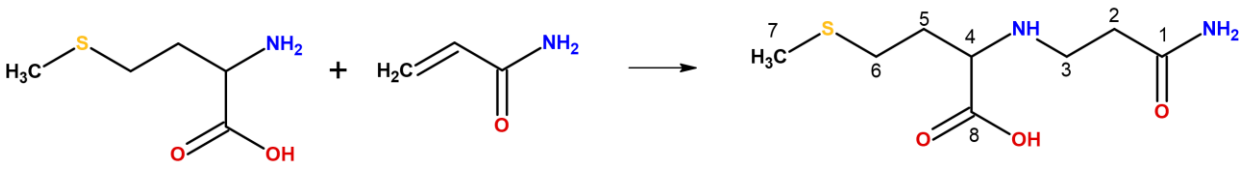

Scheme 1. Addition reaction between L-methionine and acrylamide, leading to the formation of AcryMet adduct.

The addition reaction can be monitored by NMR and Raman spectroscopies, all evidencing the disappearance of the double bond typical of the acrylamide molecule.

^{1}H and ^{13}C chemical shifts in DMSO-*d6* solution are reported in Table 1. The protons and carbons chemical shift were assigned by mono- and bi-dimensional spectra recorded at 318 K. Figure 1 shows the proton spectra, expansion 1D and 2D TOCSY, and Figure 2 the 2D hetero-correlated proton-carbon spectra HSQC (violet) and HMBC (green). HSQC correlates the carbons to directly linked protons (see Table 1). DEPT spectrum, shown as Y projection, combined with HSQC spectrum clearly displays the presence of six carbons, four methylene, one methine and one methyl groups.

The two carbonyls carbon atoms C1 (174.32 ppm) and C8 (178.57ppm) were assigned by HMBC spectrum, by mean of their long-range correlation with H2, H3 and H4, H5, respectively.

198 **Table 1.** ^{1}H and ^{13}C NMR chemical shifts for AcryMet

Atoms identification (Scheme 1)	^{1}H ppm	^{13}C ppm
1		174.32
2	2.13	35.73
3	2.49; 2.68	44.21
4	2.72	62.41
5	1.58; 1.71	33.09
6	2.46	30.33
7	2.00	14.30
8		178.57
NH	7.58	
NH_2	6.64	

199

200

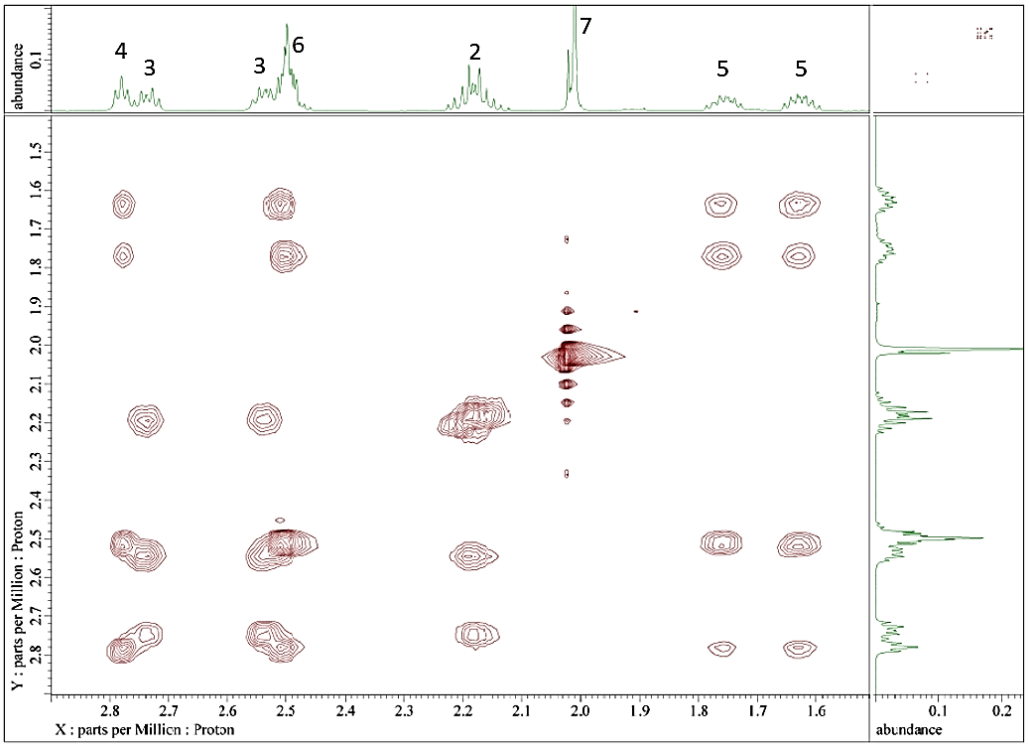

201

202 **Fig. 1.** 1D and 2D TOCSY spectra for compound AcryMet

203

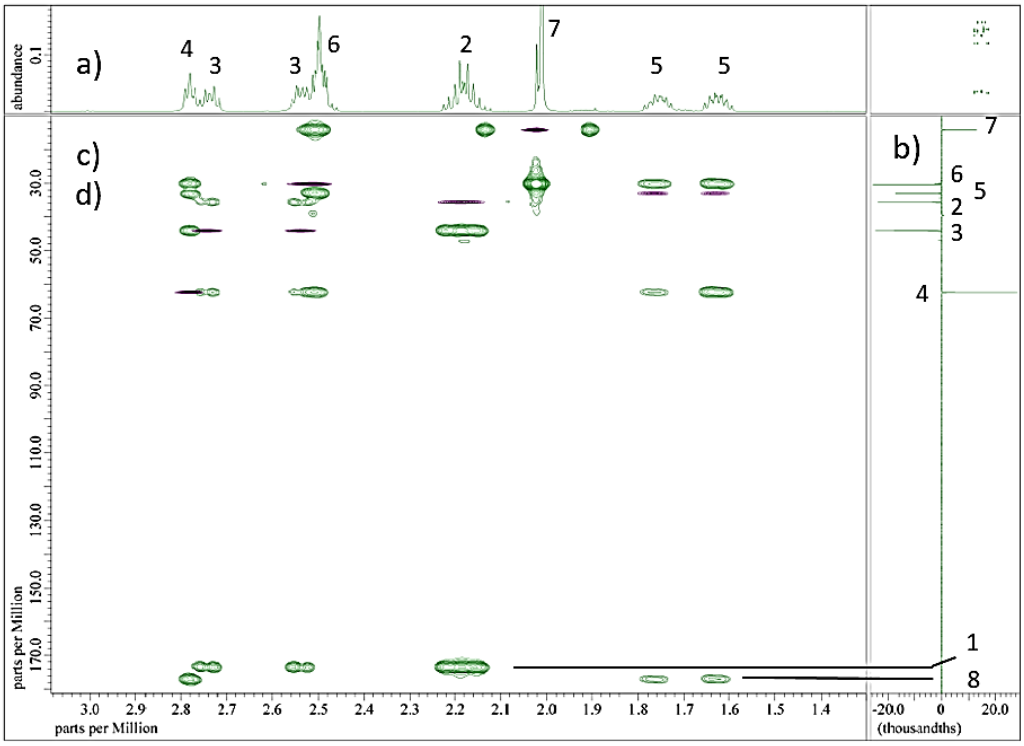

Fig. 2.1D ^{1}H (a), ^{13}C DEPT (b), 2D HSQC ((c), violet) and HMBC ((d), green) spectra for compound AcryMet.

Raman (Figure **S1**) spectra of the starting reagents and of the powdered final product AcryMet were recorded. In the Raman spectrum of acrylamide, the peaks due to vibrational modes of the amide group and of the double bond are very strong: the C=O stretching at 1681 cm^{-1}, the NH_2 deformation at 1583 cm^{-1} and the C=C stretching vibration (νC=C) at 1630 cm^{-1}. Due to the chemical changes that occur during the reaction, in the final product the amide I peak down-shifts at 1663 cm^{-1}, the amide II up-shifts to 1605 cm^{-1} and the νC=C band disappears (Bergamonti et al., 2017a; Duarte at al., 2005). confirming that the double bond addition reaction has occurred.

3.2 Crystal structure of AcryMet

The molecule presents the expected zwitterionic form in its crystalline phase (Figure 3) as evidenced by the near equal distances C-O observed in the carboxylic moiety [C8-O2 1.236(3) and C8-O1 1.248(3) Å]. The two carboxylate oxygen atoms O1 and O2 participate in strong head to tail O···H-N hydrogen

bonds with protonated $RR'NH^{2+}$ groups of adjacent molecules, and these interactions lead to a three dimensional network [N1-H1b···O1 2.714(2) Å, N1-H1b···O1 173.54(1)° and N1-H1a···O2 2.767(3) Å, N1-H1a···O2 149.64(1)°]. Moreover, the carbamoyl groups of the molecule form N-H···O hydrogen bonds within themselves, [N2-H2c···O3 3.010(3) Å, N2-H2c···O3 167.02(1)°], leading to chain linked molecules, developing along the *a* axis, as shown in Figure 4. This causes a preferred direction in the crystal growth along this axis, and the formation of needle form crystals. The molecule is enantiomeric, as derived from L-methionine and it crystallizes in a chiral space group $P2_12_12_1$ with S configuration.

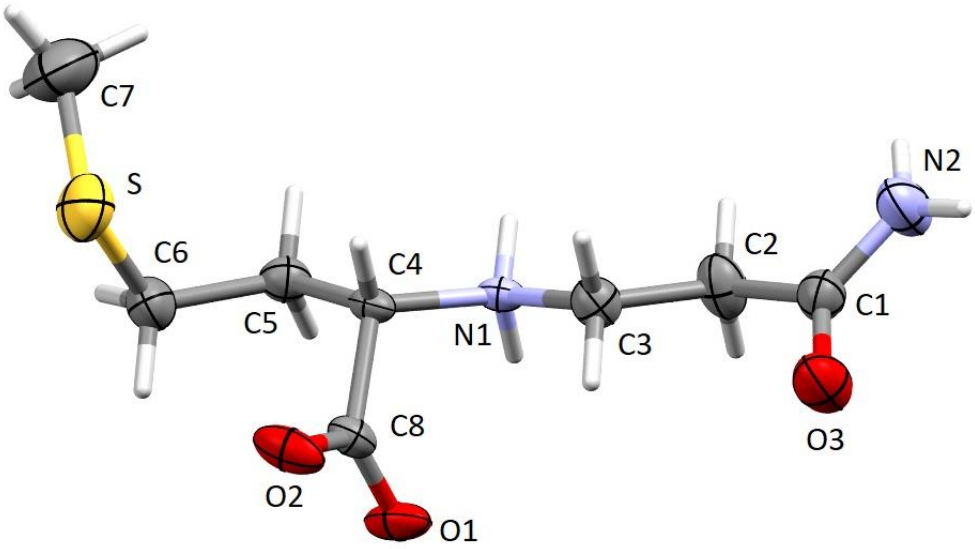

Fig. 3. Ortep view of AcryMet. Hydrogen atoms are drawn in capped stick style.

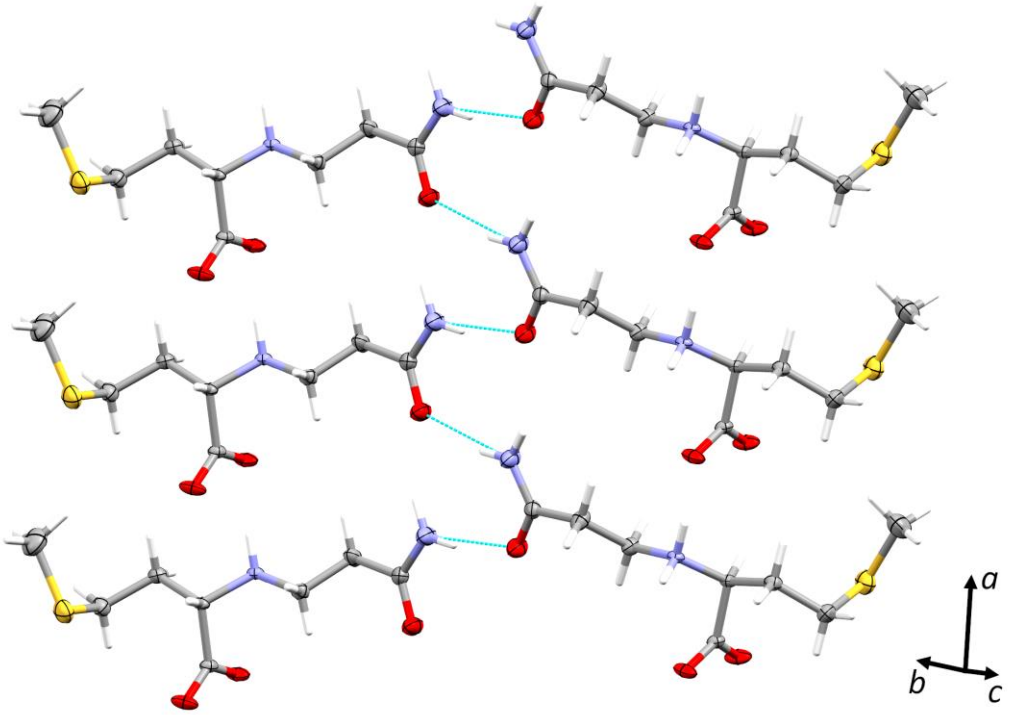

Fig. 4. Carbamoyl group forming N-H···O hydrogen bonds leading to chains linking related molecules, developing along the crystallographic *a* axis.

The anisotropic nature of the AcryMet crystals is confirmed by the Raman spectra on a single needle-like crystal taken at perpendicular orientations, as shown in figure S2. Because of hydrogen bonds play an important roles in the stability of the AcryMet crystalline structure, the main changes in the the vibrational spectrum are linked to the modes of groups involved in the H bonds, as clearly evident in the regions of the NH stretching and bending vibrations at 3150-3500 cm^{-1} and 1500-1600 cm^{-1}, respectively.

3.3 Formation of copper complex Cu^{2+}/AcryMet in solution and fully characterization in solid state

AcryMet has been reacted with Cu^{2+} cations in order to test its ability to coordinate metal ions in wastewater. In fact, the molecule presents three potential sites with high electron density, capable to coordinate to metal ions: (a) the carboxylate group, (b) the bis-amine site and, upon deprotonation, (c) the

amide carbonyl group. The study of the coordination ability can be of great interest in order to use the corresponding polymer (PAA) as active material able to sequestrate metal ions from wastewater.

The molecular view of the Cu^{2+}/AcryMet complex is shown in Figure 5. L and D enantiomers of the amido aminoacid coordinate the metal cation. Coordination of Cu^{2+} ions was reported in the literature to promote racemization of amino acids (Mathews and H. Manohar, 1991; Weinstein et al., 1970; Byun et al., 2017; Gillard and O'Brien, 1978). However, in these processes the formation of a Shiff base at the amino group makes the α-carbon more acidic. For AcryMet this is not necessary and only the presence of the copper ion induces racemization, probably for the strong interaction of the metal with the tridentate ligand.

The copper atom is placed on an inversion center and the complex shows a Jahn-Teller distorted octahedral environment, achieved by the nitrogen atom of the aminic group and the oxygen atoms of the carboxylic group on the equatorial plane, evidencing closer interactions [Cu-N1 2.008(9) Å, Cu-O1 1.909(7) Å] and of the amidic moieties of the ligand in the apical position at longer distance [Cu-O3 2.569(8) Å]. Each molecule acts as a tridentate ligand, forming a five membered chelating ring through the carboxylic and aminic groups and a six membered chelating ring through the aminic and amidic moieties; the tio-alkyl chain remains dandling and not involved in interactions. We anticipate here that 1:2 Cu^{2+}:ligand species is formed in solution for which we propose the same equatorial coordination (2 NHR, 2 COO^-) environment (see below).

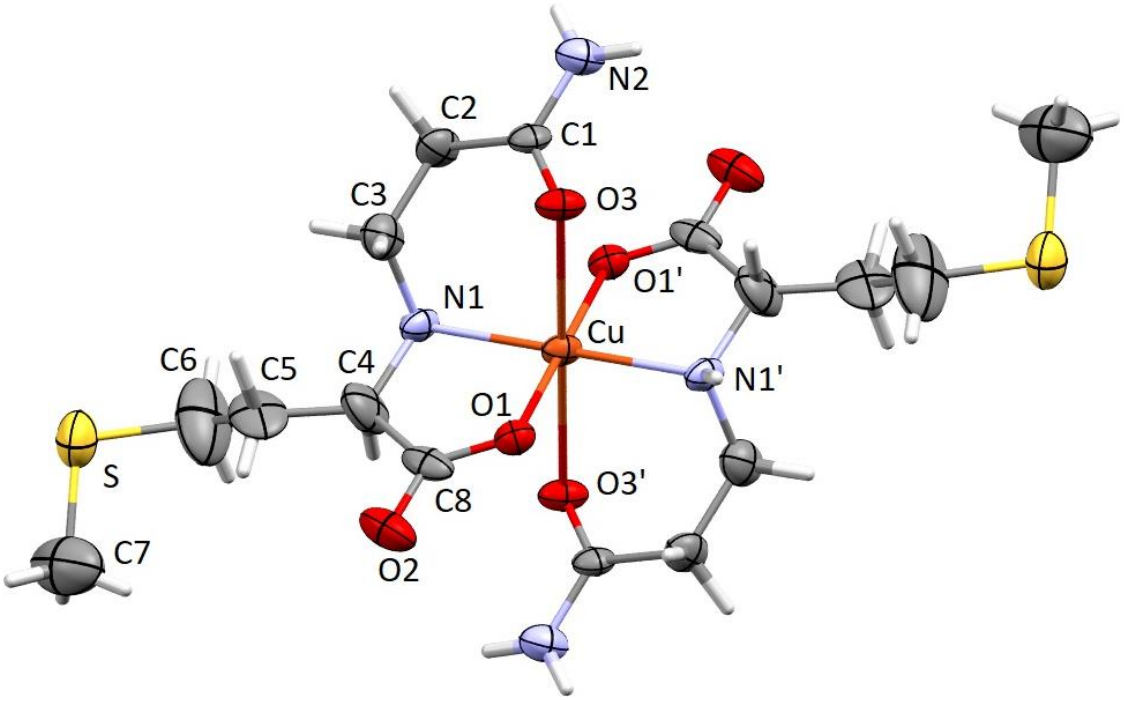

Fig. 5. Ortep view of Cu^{2+}/AcryMet Complex.

3.4 Solution equilibria

In the perspective of using AcryMet-based polymers for the extraction of metal ions from aqueous solutions, we have studied the Cu^{2+} coordination capabilities of AcryMet in water. These studies were carried out by potentiometry and UV-visible absorption spectrophotometry, and they allowed to determine the speciation of the Cu^{2+}/AcryMet system, which is reported in Table 2. The speciation of the Co^{2+}, Ni^{2+} and Zn^{2+} / AcryMet systems were determined for the sake of comparison.

Table 2. Logarithms of formation constants of the complex species of Cu^{2+}, Co^{2+}, Ni^{2+} and Zn^{2+} with AcryMet in aqueous solution (I = 0.1 M (KCl), T = 298.2 K). Visible absorption maxima of the Cu^{2+}/AcryMet species are also reported.

	Cu^{2+}		Co^{2+}	Ni^{2+}	Zn^{2+}
	log β	λ_{max} (nm)	log β	log β	log β
$[ML]^{+}$	7.99(1)	712 (717)	3.93(1)	5.52(9)	3.67(1)
$[ML_2]$	12.28(1)	628 (622)	5.99(6)	8.90(1)	5.97(7)
$[MLH_{-1}]$	0.03(1)	633 (627)	-	-5.86(7)	-
$[MLH_{-2}]^{-}$	-10.06(1)[a]	616 (592)	-	-	-
σ	1.27		2.60	2.48	3.50
n	256		139	169	144

[a] For this species we propose a $[Cu(LH_{-1})(OH)]^{-}$ stoichiometry, see text.

AcryMet in aqueous solution behaves as a biprotic ligand. In its fully protonated form (H_2L^{+}), AcryMet is protonated on both the carboxyl- and secondary amino functions. The two groups have pK_a of 1.47(2) and 7.99(1), respectively. These results confirm that AcryMet in solution is zwitterionic in its neutral form HL, in accordance with the crystal structure.

The ligand forms with Cu^{2+} four complex species: $[CuL]^{+}$, $[CuL_2]$, $[Cu(LH_{-1})]$ and $[Cu(LH_{-1})(OH)]^{-}$. The logarithms of their formation constants are reported in Table 2, and a distribution diagram is represented in Figure 6. Cu^{2+} complexation starts below pH = 3: at pH 2.4, where we started to collect potentiometric data, ca. 30 % total copper results already in the $[CuL]^{+}$ form. The $[CuL]^{+}$ complex reaches 95 % total copper at pH 4.8. The $[CuL_2]$ species starts to form at pH 5 and dominates between pH 6.8 and 9.2 with a maximum of 75% total copper at pH 8. The $[Cu(LH_{-1})]$ species starts to form at pH 7, followed by the formation of $[Cu(LH_{-1})(OH)]^{-}$. The structural models that we put forward for these species are reported in Scheme 2 and are well supported by the UV-visible absorption features that are discussed here below.

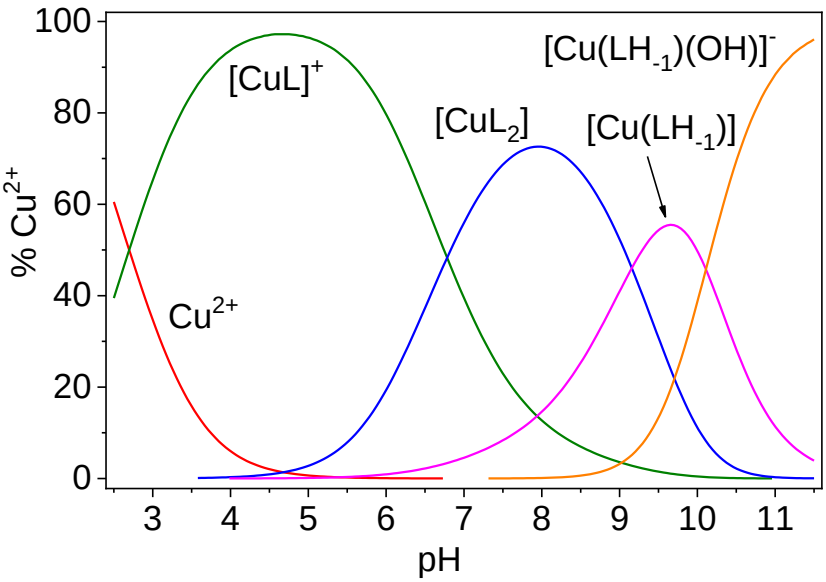

296

297 **Fig. 6.** Representative distribution diagram of the Cu^{2+}/AcryMet (HL) system (Cu:L = 1:2.2; C_{Cu} = 0.0125 M) in

298 aqueous solution. *I* = 0.1 M (KCl), *T* = 298.2 K.

299

300 Knowing the speciation system, we have investigated the Cu^{2+}/L system by UV-visible titration as a

301 function of the pH. The spectral dataset is reported in Figure **S3**. On the basis of these spectral data we

302 have calculated the UV-visible molar spectra of the Cu^{2+} species, which are reported in Figure **S4**. The

303 wavelengths corresponding to the absorption maxima of the different complex species are reported in

304 Table 2.

305 The schematic structures of the proposed equatorial coordination environment of the Cu^{2+} species

306 are represented in Scheme 2. The expected wavelengths of the absorption maxima of these species were

307 calculated using the rule of the average environment (Billo, 1974; Prenesti et al., 1999) and their values

308 are also reported in Table 2.

309

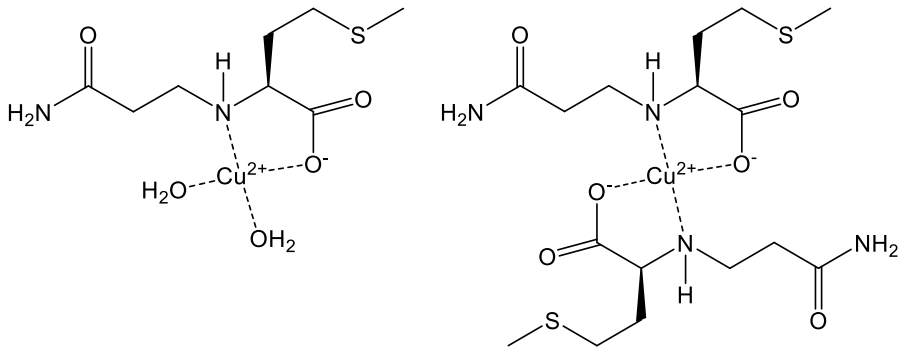

$[CuL]^+$ $[CuL_2]$

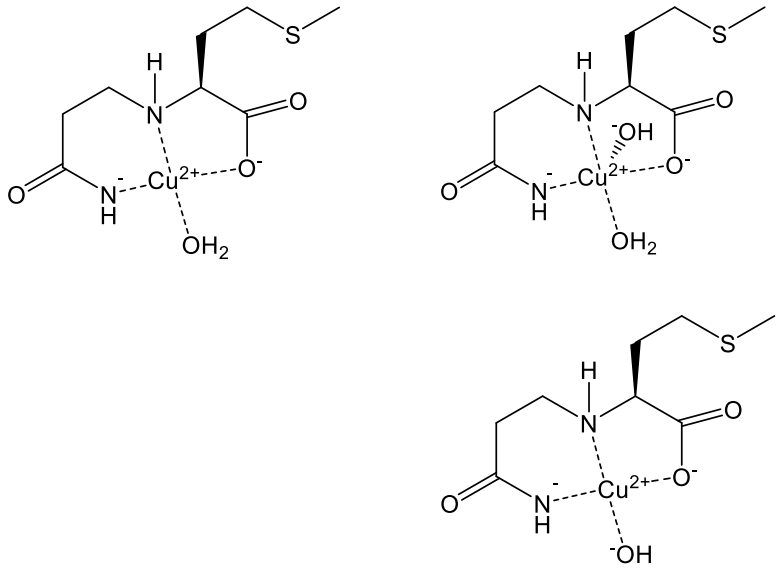

$[Cu(LH_{-1})]$ $[Cu(LH_{-1})(OH)]^-$

Scheme 2. Schematic representation of the equatorial coordination environment of the $[CuL]^+$, $[CuL_2]$, $[Cu(LH_{-1})]$ and $[Cu(LH_{-1})(OH)]^-$ species.

The evaluation of the spectral data (λ_{max} values in particular, Table 2) suggests that the AcryMet ligand acts as a bidentate (NHR, COO^-) chelating ligand in $[CuL]^+$ and $[CuL_2]$. This observation is very consistent with the crystal structure of Cu^{2+}/AcryMet. Actually, the distorted octahedral coordination of Cu^{2+} has the amino and carboxylate groups as the equatorial donor atoms, as we propose in solution for the 1:2 metal:ligand complex. Absorption data do not provide indications on the nature of the axial ligand.

Although amide oxygen atoms can coordinate to axial positions, we put forward the hypothesis that these weak interactions are rather substituted by water coordination.

At pH higher than 5 the deprotonation of the amidic nitrogen occurs, with formation of $[Cu(LH_{-1})]$, where the ligand acts as a tridentate (N^-, NHR, COO^-) chelating molecule. The deprotonation of the amidic nitrogen is prompted by the formation, in $[Cu(LH_{-1})]$, of a 5- and 6 membered chelating rings. For all three $[CuL]^+$, $[CuL_2]$, and $[Cu(LH_{-1})]$ species the observed wavelengths corresponding to the absorption maxima are consistent with the coordination modes proposed in Scheme 2.

Since no other acidic protons are present in the ligand, the highest deprotonated $[Cu(LH_{-1})(OH)]^-$ species corresponds to an hydroxo-coordinated complex (Scheme 2). Spectroscopic and potentiometric data suggest that a mixture of axially- and equatorially-deprotonated water molecules are present, or more likely a distorted species which is structurally intermediate between the two geometries. On one hand, the pK_a of the $[Cu(LH_{-1})] = [Cu(LH_{-1})(OH)]^- + H^+$ process results -10.03(1). This value is intermediate between that of [CuL] of trien (10.7) where the deprotonation of an axial water molecule takes place, and that of [CuL] of dien (9.1) where the deprotonation is certainly on the equatorial plane (Smith et al., 2007). Also, should the deprotonation of $[Cu(LH_{-1})]$ occur on the equatorial plane, a blue shift to ca. 595 nm is expected on the basis of the Billo's parameters (Prenesti et al., 1999). Conversely, a small red shift is expected for the formation of an axially-coordinated hydroxo-complex (Sigel and Martin, 1982). Therefore, the experimental λ_{max} of 616 nm determined for $[Cu(LH_{-1})(OH)]^-$ is intermediate between the spectral shifts expected for the deprotonation of $[Cu(LH_{-1})]$ into either an axially- and an equatorially-bound hydroxide. One last experimental evidence for the presence of an intermediate axial-equatorial hydroxo-species relates with the spectrum bandwidth. The calculated spectra in Figure **S5** show no appreciable broadening effect or maximum splitting for the calculated spectrum of $[Cu(LH_{-1})(OH)]^-$ compared to those of the other species. In this respect, if two different species absorbing at ca. 595 and 620 nm, respectively, are present in solution, a significant band broadening should be observed. This was not evidenced experimentally, and therefore we conclude that $[Cu(LH_{-1})(OH)]^-$ corresponds to one single species geometrically intermediate between and axially- and an equatorially- hydroxo-complex.

Potentiometric and spectrophotometric studies were carried out also on the Ni^{2+}, Co^{2+} and Zn^{2+}/AcryMet systems. In particular we determined the stability of the complexes of Ni^{2+} and Co^{2+} with the purpose of finding conditions that allow to control their binding to the ligand. Logarithms of complex formation constants are reported in Table 2, while representative speciation diagrams are reported as supporting information. Spectra dataset for the UV-vis characterization of systems containing Ni^{2+} and Co^{2+} as a function of the pH are also reported as supporting info. For all three cations both $[ML]^+$ and $[ML_2]$ species form in solution. For Ni^{2+}, a small amount of $[Ni(LH_{-1})]$ is also formed at high pH values. For all these complexes, the proposed coordination modes of AcryMet in solution are analogous to those of the complexes of Cu^{2+}, considering the species with the same stoichiometry.

Quite expectedly, data in Table 2 (e.g. log β of $[ML]^+$ or $[ML_2]$ species) evidence that the order of the global formation constants reflects the Irving-Williams series, (i.e. $Co^{2+} < Ni^{2+} < Cu^{2+} > Zn^{2+}$). This behavior is also reflected into the pH at which, for instance, the $[ML]^+$ species is formed. Cu^{2+} forms the most stable complexes, and in fact 30% total copper is already in the $[CuL]^+$ form at pH 2.5. On the contrary, Ni^{2+} complexes start to form at pH 3.5, Co^{2+} species at pH 3.5, and Zn^{2+} species at pH 5.5. It is therefore clear that through a wise choice of the pH conditions of the medium it is possible to obtain solely Cu^{2+} coordinated to the ligand (low pH), or Cu^{2+} and Ni^{2+} (intermediate pH), or all three Cu^{2+}, Ni^{2+} and Co^{2+} cations (high pH).

In the perspective of using AcryMet-based polymers to sequester toxic transition metal ions from water, we have therefore calculated a competition distribution diagram for a theoretical $Co^{2+}/Ni^{2+}/Cu^{2+}$/MAA (HL) = 1:1:1:3 system, represented in Figure **S6-11**. In this system, L is expected to bind almost selectively Cu^{2+} at pH below 4. Between pH 4 and 6, binding of both Cu^{2+} and Ni^{2+} is expected, while complexation of Co^{2+} occurs at pH higher than 6. To prove experimentally this sequential binding behavior, we carried out a pH-spectrophotometric titration of a sample containing equimolar amounts of Cu^{2+}, Ni^{2+} and Co^{2+}, and 3 equivalents of AcryMet. Starting from pH 2.8 we increased the pH by addition of a solution of KOH until pH 8.8. The absorption spectrum in the visible range was collected at intervals of pH of ca. 0.3 units. The spectral dataset is reported in Figure 7. At pH 2.8 the maximum of

absorption is 715 nm, and the intensity of this band increases until pH 4.5. This absorption maximum corresponds to that of $[CuL]^+$ (see above), and the increase of absorbance follows the increase of $[CuL]^+$ formation as expected from the Cu^{2+} distribution diagram. This intense band shifts at pH higher than 5 to ca. 650 nm as a consequence of the formation of $[Cu(LH_{-1})]$ and $[CuL_2]$.

Interestingly, the absorbance at ca. 900 nm remains low until pH 4.1 and it increases at higher pH values. The absorption of the Cu^{2+} species at this wavelength tends to decrease above pH 4.5, and therefore the increase of intensity at ca. 900 nm is clearly ascribed at the formation of $[NiL]^+$ which in fact occurs at pH > 4. The low molar absorption of Co^{2+} species did not allow to detect their formation as well defined bands. However, the shoulder at ca. 500-550 nm increases markedly above pH 6, and this change cannot be associated to either Cu^{2+} or Ni^{2+} species which provide a limited spectral change at those wavelengths. Rather, the formation of $[CoL]^+$ which occurs at pH > 6 explains this quite significant change in the absorption of the shoulder. Overall, these results demonstrate experimentally a sequential complexation of these divalent metal ions in aqueous solution by AcryMet.

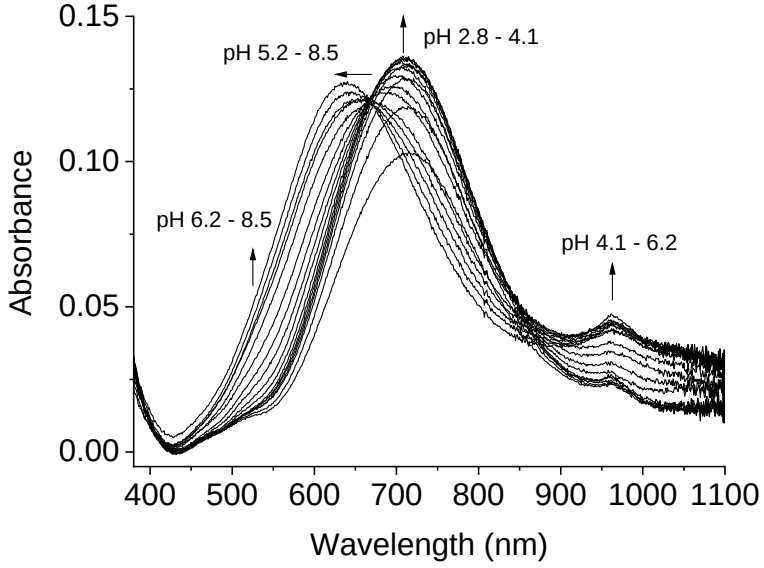

Fig. 7. UV-visible absorption spectra of the system Cu^{2+} / Ni^{2+} / Co^{2+} / AcryMet (HL) at different pH values in aqueous solution. Cu:Ni:Co:L = 1:1:1:3, $C_{Cu,Ni,Co}$= 0.00183 M, *I*= 0.1 M KCl, *T* = 298.2 K, d= 1 cm, pH range = 2.8-8.5.

Finally, we have used out equilibrium data to simulate what is the capacity of our ligand to bind metal ions Cu(II), Ni(II) and Co(II) at 1.6 10^{-3} M (1 ppm) concentration each, and a ligand/total metal content = 1.25:1. The results are reported in Figure S12. Free (uncomplexed) copper at pH 2.5 amounts to 40 %, and total complexation is obtained at pH ca. 4.5. Moreover, Ni(II) results almost entirely complexed at pH 7. Co(II) is the only cation for which no complete complexation is obtained in the pH range 2.5-8. However, at pH 8 less than 50 % total Co(II) is in its free form. Overall these data demonstrate that, at least for Cu(II) and Ni(II), the sequestration capacity of the ligand toward the metal ions is relevant also in trace levels.

3.5 Metal Ions Adsorption

The kinetic experimental curves, C_t (mg/L) versus t (min) for Cu(II), Co(II) and Ni (II), are shown in Fig. 8. The removal of metal due to adsorption is high during the first 180 min for all metal ions. Then, it gradually decreases until equilibrium at 300 min. The rapid adsorption of metal ions in the first three hours may be favored by the presence of several binding sites of the Acry-Met ligand which are available for the adsorption of these intermediate (hard-soft) cations. With the progress of the experiment, the concentration of metals and binding sites decrease, causing a slowdown of the adsorption.

The pseudo-first-order kinetics model by Lagergren model [eq. 3] was used to describe the adsorption kinetics of Cu(II), Co(II) and Ni(II) ions onto the Acry-Met film:

$$q_t = q_e\ (1 - esp^{k_1 t}) \qquad (3)$$

where q_t and q_e (mg g^{-1}) are the amounts of metal adsorbed at time t and at the equilibrium time, respectively, and k_1 (min^{-1}) is the pseudo-first-order model rate constant.

412 Kinetic parameters of pseudo-first-order, obtained from the plot of experimental curves (Fig. 8), and the
413 results are presented in Table 3

414 **Table 3**. Kinetic parameters of metal sorption onto the Acry-Met.

Metal	q_e (mg/g)	R_{ads} (%)	*Pseudo first order model*	
			k_1 x 10^{-3} (min^{-1})	R^2
Cu(II)	1.57	63	0.07	96
Co(II)	1.14	46	0.05	99
Ni(II)	0.89	36	0.04	97

415

416 Overall, data in Table 3 show a membrane loaded with Acry-Met, even if the latter is just dispersed in
417 TEOSs with no precise control of the reticulation of the material, is efficient to remove these two metal
418 ions from the bulk of the solution. Cu(II) presents the highest amount of metal absorbed qe parameter and
419 the highest rate constant among the three examined. This is perhaps expected for the metal which is
420 highest in the Irving-William series, and which present high rates of substitution of coordinated ligands.

421

422 **4. Conclusions**

423 The removal of toxic metal ions from wastewater is one of the most important targets of current
424 research due to the harmful effects that this kind of pollutants can produce on the human health and
425 environment. In this work the synthesis and characterization of the AcryMet ligand has been presented,
426 together with the X-ray characterization of a 1:2 Cu^{2+}/ligand complex. The study of the speciation of
427 divalent cations and especially Cu^{2+}, Ni^{2+} and Co^{2+} / AcryMet systems is reported and discussed.

428 AcryMet is the monomeric analogue of the building blocks that constitute polyamidoaminic materials
429 that we have previously reported in the literature. Here we have demonstrated that the complexation of
430 divalent cations basically pivots around the presence of the secondary amine. Further interactions with
431 the metal ions, as clearly proved for Cu^{2+}, occurs by the involvement of the carboxylate function and, at

high pH, of the deprotonated amidic nitrogen. Perhaps most importantly, the presence of the deprotonated acidic group close to secondary amine in AcryMet is responsible of the sequential binding behavior of the ligand. Actually, the ligand forms complexes with Cu^{2+} at pH around 2.5-3 by virtue of the presence of this deprotonated carboxylic function. The complexation of Ni^{2+} starts at pH > 3.5 while that of Co^{2+} only occurs at pH > 6.

Transferred at the polymer level, these observations suggest that metal ions may interact at the secondary amino groups also with the corresponding PAA. Additional interactions may occur at the deprotonated amidic nitrogen where the flexibility of the polymeric chains and the pH conditions allow it. Also, depending on the monomeric components used to prepare the polymers, we may observe the interaction of metal ions with carboxylate functions close to secondary amines. We hope in the future not only to transfer the metal coordination capability of AcryMet into a polymeric material, but also to impart the same material with sequential-binding complexation capabilities. The latter will be extremely interesting in the perspective of sequestration and release of divalent metal cations from water samples, which may occur with sequential selection by simply changing the pH of the solution.

Acknowledgment

The authors are gratefully acknowledged to Prof. Giovanni Predieri for useful discussion and Dr.ssa Viviana Dattaro for experimental work during her degree thesis. This work has benefited from the equipment and framework of the COMP-HUB Initiative, funded by the 'Departments of Excellence' program of the Italian Ministry for Education, University and Research (MIUR, 2018-2022).

References

Alberti, G., Mussi, M., Quattrini, F., Pesavento, M., & Biesuz, R. (2018). Metal complexation capacity of Antarctic lacustrine sediments. Chemosphere, 196, 402-408. https://doi.org/10.1016/j.chemosphere.2017.12.188

Alderighi, L., Gans, P., Ienco, A., Peters, D., Sabatini, A., Vacca, A., 1999. Hyperquad simulation and speciation (HySS): a utility program for the investigation of equilibria involving soluble and partially soluble species. Coordination chemistry reviews, 184(1), 311-318. https://doi.org/10.1016/S0010-8545(98)00260-4

Bailey, S. E., Olin, T. J., Bricka, R. M., Adrian, D. D., 1999. A review of potentially low-cost sorbents for heavy metals. *Water research*, *33*(11), 2469-2479. https://doi.org/10.1016/S0043-1354(98)00475-8

Barbucci, R., Barone, V., Ferruti, P., Delfini, M., 1980. Macro-inorganics. Part 3. Chelation of copper (II) ion with some polymers having a poly (amido-amine) structure and their non-macromolecular models. *Journal of the Chemical Society, Dalton Transactions*, (2), 253-256. https://doi.org/10.1039/DT9800000253

Bergamonti, L., Graiff, C., Tegoni, M., Predieri, G., Bellot-Gurlet, L., Lottici, P. P., 2017a. Raman and NMR kinetics study of the formation of amidoamines containing N-hydroxyethyl groups and investigations on their Cu (II) complexes in water. *Spectrochimica Acta Part A: Molecular and Biomolecular Spectroscopy*, *171*, 515-524. https://doi.org/10.1016/j.saa.2016.07.041

Bergamonti, L., Berzolla, A., Chiappini, E., Feci, E., Maistrello, L., Palanti, S., ... Vaccari, G., 2017b. Polyamidoamines (PAAs) functionalized with siloxanes as wood preservatives against fungi and insects. *Holzforschung*, *71*(1), 65-75. https://doi.org/10.1515/hf-2016-0010

Bergamonti, L., Graiff, C., Tegoni, M., Predieri, G., Elviri, L., Palanti, S., ... Lottici, P. P., 2019. Facile preparation of functionalized poly (amidoamine) s with biocidal activity on wood substrates. *European Polymer Journal*, *116*, 232-241. https://doi.org/10.1016/j.eurpolymj.2019.04.027

Betiha, M. A., Moustafa, Y. M., El-Shahat, M. F., & Rafik, E. (2020). Polyvinylpyrrolidone-Aminopropyl-SBA-15 schiff Base hybrid for efficient removal of divalent heavy metal cations from wastewater. *Journal of Hazardous Materials*, 122675. https://doi.org/10.1016/j.jhazmat.2020.122675

Billo, E. J., 1974. Copper (II) chromosomes and the rule of average environment. *Inorganic and Nuclear Chemistry Letters*, *10*(8), 613-617. https://doi.org/10.1016/0020-1650(74)80002-4

Bo, S., Luo, J., An, Q., Xiao, Z., Wang, H., Cai, W., ... Li, Z., 2020. Efficiently selective adsorption of Pb (II) with functionalized alginate-based adsorbent in batch/column systems: Mechanism and application simulation. *Journal of Cleaner Production*, 250, 119585. https://doi.org/10.1016/j.jclepro.2019.119585

Brahmi, K., Bouguerra, W., Harbi, S., Elaloui, E., Loungou, M., & Hamrouni, B. (2018). Treatment of heavy metal polluted industrial wastewater by a new water treatment process: ballasted electroflocculation. *Journal of Hazardous Materials*, 344, 968-980. https://doi.org/10.1016/j.jhazmat.2017.11.051

Bruker, 2015. APEX3 and SAINT. Bruker AXS Inc., Madison, Wisconsin, USA

Byun, I. S., Han, K. S., Ga, H. R., 2017. Process for the racemization of α-amino acids. U.S. Patent No. 9,598,353. Washington, DC: U.S. Patent and Trademark Office.

Casolaro, M., Bignotti, F., Sartore, L., Penco, M., Ferruti, P., 1998. Stability of metal complexes with basic polymers in the free, cross-linked and silica-grafted forms. *Current Trends in Polymer Science*., 3, 173-182.

Chandrarekha, M., Srinivasan, N., Krishnakumar, R. V., 2015. Redetermined crystal structure of N-(β-carboxyethyl)-α-isoleucine. *Acta Crystallographica Section E: Crystallographic Communications*, 71(9), o665-o666. https://doi.org/10.1107/S2056989015014498

Esshaimi, M., Ouazzani, N., Avila, M., Perez, G., Valiente, M., & Mandi, L. (2012). Heavy metal contamination of soils and water resources Kettara abandoned mine. American Journal of Environmental Sciences, 8(3), 253-261. https://doi.org/10.3844/ajessp.2012.253.261

Duarte A.S.R., Amorim Da Costa A.M, Amado A.M., 2005. On the conformation of neat acrylamide dimers - a study by ab initio calculations and vibrational spectroscopy, *Journal of Molecular Structure: THEOCHEM* 723, 63–68, http://dx.doi.org/10.1016/j.theochem.2005.02.008.

Farrugia, L. J., 2012. WinGX and ORTEP for Windows: an update. *Journal of Applied Crystallography*, *45*(4), 849-854. https://doi.org/10.1107/S0021889812029111

Febrianto, J., Kosasih, A. N., Sunarso, J., Ju, Y. H., Indraswati, N., Ismadji, S., 2009. Equilibrium and kinetic studies in adsorption of heavy metals using biosorbent: a summary of recent studies. *Journal of Hazardous Materials*, 162(2-3), 616-645. https://doi.org/10.1016/j.jhazmat.2008.06.042

Ferruti P., 2013. Poly(amidoamine)s: Past, Present, and Perspectives *Journal of Polymer Science, Part A: Polymer Chemistry*, *51*, 2319–2353, https://doi.org/10.1002/pola.26632

Ferruti, P., Danzo, N., Oliva, L., Barbucci, R., Barone, V., 1981. Macro-inorganics. Part 6. Protonation and complex formation of a new series of polymers whose repeating units behave independently. *Journal of the Chemical Society, Dalton Transactions*, (2), 539-542. https://doi.org/10.1039/DT9810000539

Ferruti, P., Marchisio, M. A., Duncan, R., 2002. Poly (amido-amine) s: Biomedical Applications. *Macromolecular Rapid Communications, 23(5-6),* 332-355. http://dx.doi.org/10.1002/1521-3927(20020401)23:5/6b332::AID-MARC332N3.0.CO;2-I

Ferruti, P., Mauro, N., Falciola, L., Pifferi, V., Bartoli, C., Gazzarri, M., ... Ranucci, E., 2014. Amphoteric, Prevailingly Cationic l-A rginine Polymers of Poly (amidoamino acid) Structure: Synthesis, Acid/B ase Properties and Preliminary Cytocompatibility and Cell-P ermeating Characterizations. *Macromolecular bioscience, 14(3),* 390-400. https://doi.org/10.1002/mabi.201300387

Ferruti, P., Oliva, L., Barbucci, R., Tanzi, M. C., 1980. Macro inorganics V. Basicity and complexing ability of a new class of poly (amido-amines) with tertiary amino groups present both in the main chain and as side substituent. *Inorganica Chimica Acta, 41*, 25-29. https://doi.org/10.1016/S0020-1693(00)88426-1

Ferruti, P., Ranucci, E., Manfredi, A., Mauro, N., Ferrari, E., Bruni, R., ... Rossi, M., 2012. L-lysine and EDTA polymer mimics as resins for the quantitative and reversible removal of heavy metal ion water pollutants. *Journal of Polymer Science Part A: Polymer Chemistry, 50(24),* 5000-5010. https://doi.org/10.1002/pola.26330

Fu, F., Wang, Q., 2011. Removal of heavy metal ions from wastewaters: a review. *Journal of environmental management, 92*(3), 407-418. https://doi.org/10.1016/j.jenvman.2010.11.011

Gans, P., Sabatini, A., Vacca, A., 1996. Investigation of equilibria in solution. Determination of equilibrium constants with the HYPERQUAD suite of programs. *Talanta-Oxford, 43*(10), 1739-1754. https://doi.org/10.1016/0039-9140(96)01958-3

Gillard, R. D., P. O'Brien, 1978. The isomers of α-amino-acids with copper (II). Part 4. Catalysis of the racemization of optically active alanine by copper (II) and pyruvate in alkaline solution. *Journal of the Chemical Society, Dalton Transactions* 11, 1444-1447. https://doi.org/10.1039/DT9780001444

Girardi, F., Bergamonti, L., Isca, C., Predieri, G., Graiff, C., Lottici, P. P., ... Di Maggio, R., 2017. Chemical–physical characterization of ancient paper with functionalized polyamidoamines (PAAs). *Cellulose, 24(2),* 1057-1068. https://doi.org/10.1007/s10570-016-1159-8

Hurd, R. E., 1990. Gradient-enhanced spectroscopy. *J. Magn. Reson., 87,* 422-428. https://doi.org/10.1016/0022-2364(90)90021-Z

Isca, C., D'Avorgna, S., Graiff, C., Montanari, M., Ugozzoli, F., Predieri, G., 2016. Paper preservation with polyamidoamines: a preliminary study. *Cellulose, 23(2),* 1415-1432. http://dx.doi.org/10.1007/s10570-016-0880-7

546 Joseph, L., Jun, B. M., Flora, J. R., Park, C. M., & Yoon, Y., 2019. Removal of heavy metals from water
547 sources in the developing world using low-cost materials: A review. *Chemosphere*, *229*, 142-159.
548 https://doi.org/10.1016/j.chemosphere.2019.04.198

549 Ju, S., Eom, Y., Kim, S. Y., Hwang, S. Y., Hwang, D. S., Oh, D. X., Park, J., 2019. Lysine-cyclodipeptide-
550 based polyamidoamine microparticles: Balance between the efficiency of copper ion removal and
551 degradation in water. *Chemical Engineering Journal*, 123493. https://doi.org/10.1016/j.cej.2019.123493

552 Lachowicz, J. I., Crespo-Alonso, M., Caltagirone, C., Alberti, G., Biesuz, R., Orton, J. O., & Nurchi, V.
553 M. (2018). Salicylamide derivatives for iron and aluminium sequestration. From synthesis to
554 complexation studies. Journal of Trace Elements in Medicine and Biology, 50, 580-588.
555 https://doi.org/10.1016/j.jtemb.2018.04.010

556 Lakherwal, D., 2014. Adsorption of heavy metals: a review. *International journal of environmental*
557 *research and development*, *4*(1), 41-48. http://www.ripublication.com/ijerd.htm

558 Lee, K. M., Lai, C. W., Ngai, K. S., Juan, J. C., 2016. Recent developments of zinc oxide based
559 photocatalyst in water treatment technology: a review. *Water research*, *88*, 428-448.
560 https://doi.org/10.1016/j.watres.2015.09.045

561 Levitt, M. H.; Freeman, R.; Frenkiel, T., 1982. Broadband heteronuclear decoupling. *Journal of Magnetic*
562 *Resonance (1969)*, *47*, 328-330. https://doi.org/10.1016/0022-2364(82)90124-X

563 Li, T., Zhang, W., Zhai, S., Gao, G., Ding, J., Zhang, W., ... Lv, L., 2018. Efficient removal of nickel (II)
564 from high salinity wastewater by a novel PAA/ZIF-8/PVDF hybrid ultrafiltration membrane. *Water*
565 *research*, 143, 87-98. https://doi.org/10.1016/j.watres.2018.06.031

566 Lim, M. C., Chen, W., Ali, H. M., 1994. Crystal and molecular structures of bis (N-propionamido-
567 glycinato) copper (II) hydrate, bis (N, N-dipropionamido-glycinato) copper (II) dihydrate and bis (N, N-
568 dipropionamido-glycinato)-μ-carboxylato-dicopper (II) perchlorate hydrate. *Transition Metal Chemistry*,
569 *19(4)*, 409-412. https://doi.org/10.1007/BF00139316

570 Malik, L. A., Bashir, A., Qureashi, A., & Pandith, A. H., 2019. Detection and removal of heavy metal
571 ions: a review. *Environmental Chemistry Letters*, 1-27. https://doi.org/10.1007/s10311-019-00891-z

572 Manfredi, A., Mauro, N., Terenzi, A., Alongi, J., Lazzari, F., Ganazzoli, F., ... Ferruti, P., 2017. Self-
573 ordering secondary structure of D-and L-arginine-derived polyamidoamino acids. *ACS Macro Letters, 6(9)*, 987-991. https://doi.org/10.1021/acsmacrolett.7b00492

575 Manfredi, A., Ranucci, E., Morandi, S., Mussini, P. R., Ferruti, P., 2013. Fast and quantitative manganese
576 sorption by polyamidoamine resins. *Journal of Polymer Science Part A: Polymer Chemistry, 51(4)*, 769-
577 773. https://doi.org/10.1002/pola.26462

578 Marcovecchio, J.E., Botté, S.E., Freije, R. H., 2007. Heavy metals, major metals, trace elements.
579 *Handbook of water analysis, 2*, 275-311.

580 Mathews, I.I., Manohar H., 1991) A novel amino acid racemization in vitamin b6-amino acid schiff base
581 copper complexes: crystal structures of aquo (5′-phosphopyridoxylidene-dl-tyrosinato) copper (II) 3.5
582 H_2O and aquo (5′-phosphopyridoxylidene-dl-phenylalaninato) copper (II) 2.5 H_2O. *Polyhedron* 10.18
583 2163-2169. https://doi.org/10.1016/S0277-5387(00)86136-7

584 Nasir A.M., Goh P.S., Abdullah M.S., Cheer N.B., Ismail A.F., 2019. Adsorptive nanocomposite
585 membranes for heavy metal remediation: Recent progresses and challenges. *Chemosphere 232*, 96e112.
586 https://doi.org/10.1016/j.chemosphere.2019.05.174

587 Nehls, I., Hanebeck, O., Becker, R., Emmerling, F., 2013. N-(β-Carboxyethyl)-α-isoleucine. *Acta*
588 *Crystallographica Section E: Structure Reports Online, 69(2),* o172-o173.
589 https://doi.org/10.1107/S160053681205146X

590 Pan, B., Zhang, Q., Du, W., Zhang, W., Pan, B., Zhang, Q., ... & Zhang, Q., 2007. Selective heavy metals
591 removal from waters by amorphous zirconium phosphate: Behavior and mechanism. *Water*
592 *Research, 41*(14), 3103-3111. https://doi.org/10.1016/j.watres.2007.03.004

Prenesti, E., Daniele, P. G., Prencipe, M., Ostacoli, G., 1999. Spectrum–structure correlation for visible absorption spectra of copper (II) complexes in aqueous solution. *Polyhedron*, *18*(25), 3233-3241. https://doi.org/10.1016/S0277-5387(99)00279-X

Quaretti, M., Porchia, M., Tisato, F., Trapananti, A., Aquilanti, G., Damjanović, M., ... Tegoni, M., 2018. Thermodynamic stability and structure in aqueous solution of the $[Cu(PTA)_4]^+$ complex (PTA= aminophosphine-1, 3, 5-triaza-7-phosphaadamantane). *Journal of inorganic biochemistry*, *188*, 50-61. https://doi.org/10.1016/j.jinorgbio.2018.08.008

Rajalakshmi, V., Vijayaraghavan, V. R., Varghese, B., Raghavan, A., 2008. Novel Michael addition products of bis (amino acidato) metal (II) complexes: Synthesis, characterization, dye degradation, and oxidation properties. *Inorganic chemistry*, *47(13)*, 5821-5830. https://doi.org/10.1021/ic800086y

Rezania, S., Taib, S. M., Din, M. F. M., Dahalan, F. A., Kamyab, H., 2016. Comprehensive review on phytotechnology: heavy metals removal by diverse aquatic plants species from wastewater. *Journal of Hazardous Materials*, *318*, 587-599. https://doi.org/10.1016/j.jhazmat.2016.07.053

Rinaldi, P. L.; Keifer, P. A., 1994. The utility of pulsed-field gradient HMBC for organic structure determination. *Journal of Magnetic Resonance, Series A*, 108, 259-262. https://doi.org/10.1006/jmra.1994.1121

Sheldrick, G. M., 2015. Crystal structure refinement with SHELXL. *Acta Crystallographica Section C: Structural Chemistry*, *71*(1), 3-8. https://doi.org/10.1107/S2053229614024218

Smith, R. M.; Martell, A. E.; Motekaitis, R. J. NIST Critically Selected Stability Constants of Metal Complexes Database. NIST: Gaithersburg, MD, USA 2007

Sigel, H., Martin, R. B., 1982. Coordinating properties of the amide bond. Stability and structure of metal ion complexes of peptides and related ligands. *Chemical Reviews*, *82*(4), 385-426. https://doi.org/10.1021/cr00050a003

Tahir, M.B., Kiran, H. Iqbal, T., 2019. The detoxification of heavy metals from aqueous environment using nano-photocatalysis approach: a review. *Environmental Science and Pollution Research 26,* 10515. https://doi.org/10.1007/s11356-019-04547-x

Tarazona-Vasquez, F., Balbuena, P. B., 2005. Complexation of Cu (II) ions with the lowest generation poly (amido-amine)-OH dendrimers: a molecular simulation study. *The Journal of Physical Chemistry B, 109(25),* 12480-12490. http://dx.doi.org/10.1021/jp051469p.

Uddin, M. K., 2017. A review on the adsorption of heavy metals by clay minerals, with special focus on the past decade. *Chemical Engineering Journal*, 308, 438-462. https://doi.org/10.1016/j.cej.2016.09.029

Vardhan, K. H., Kumar, P. S., and Panda, R. C., 2019. A review on heavy metal pollution, toxicity and remedial measures: Current trends and future perspectives. *Journal of Molecular Liquids*, *290*, 111197. https://doi.org/10.1016/j.molliq.2019.111197

Vareda, J. P., Valente, A. J., and Durães, L., 2019. Assessment of heavy metal pollution from anthropogenic activities and remediation strategies: A review. *Journal of environmental management*, *246*, 101-118. https://doi.org/10.1016/j.jenvman.2019.05.126

Wadhawan, S., Jain, A., Nayyar, J., Mehta, S. K., 2020. Role of nanomaterials as adsorbents in heavy metal ion removal from waste water: A review. *Journal of Water Process Engineering*, *33*, 101038. https://doi.org/10.1016/j.jwpe.2019.101038

Wang, L., Luo, Y., Li, H., Yu, D., Wang, Y., Wang, W., Wu, M., 2020. Preparation and selective adsorption of surface-imprinted microspheres based on hyperbranched polyamide–functionalized sodium alginate for the removal of Sb (III). *Colloids and Surfaces A: Physicochemical and Engineering Aspects*, 585, 124106. https://doi.org/10.1016/j.colsurfa.2019.124106

Weinstein, G. N., M. J. O'connor, R. H. Holm., 1970) Preparation, properties, and racemization kinetics of copper (II)-Schiff base-amino acid complexes related to vitamin B6 catalysis. *Inorganic Chemistry*, *9.9* 2104-2112. https://doi.org/10.1021/ic50091a029

Wilker, W.; Leibfritz, D.; Kerssebaum, R.; Bermel, W., 1993. Gradient selection in inverse heteronuclear correlation spectroscopy. *Magnetic Resonance in Chemistry*, *31*, 287-292. https://doi.org/10.1002/mrc.1260310315

Xiaoli, C., Shimaoka, T., Xianyan, C., Qiang, G., & Youcai, Z. (2007). Characteristics and mobility of heavy metals in an MSW landfill: Implications in risk assessment and reclamation. *Journal of hazardous materials*, 144(1-2), 485-491. https://doi.org/10.1016/j.jhazmat.2006.10.056

Xu, Y., Zhao, D., 2005. Removal of copper from contaminated soil by use of poly (amidoamine) dendrimers. *Environmental science technology, 39(7),* 2369-2375. http://dx.doi.org/10.1021/es040380e

Zheng, X., Liu, T., Guo, M., Li, D., Gou, N., Cao, X., ... & Pan, B., 2020. Impact of heavy metals on the formation and properties of solvable microbiological products released from activated sludge in biological wastewater treatment. *Water Research*, 115895. https://doi.org/10.1016/j.watres.2020.115895

Zhou, G., Luo, J., Liu, C., Chu, L., & Crittenden, J. (2018). Efficient heavy metal removal from industrial melting effluent using fixed-bed process based on porous hydrogel adsorbents. *Water research*, *131*, 246-254. https://doi.org/10.1016/j.watres.2017.12.067

Zintchenko, A., van der Aa, L. J., Engbersen, J. F., 2011. Improved synthesis strategy of poly (amidoamine) s for biomedical applications: catalysis by "green" biocompatible earth alkaline metal salts. *Macromolecular rapid communications, 32(3),* 321-325. http://dx.doi.org/10.1002/marc.201000545